Niemeyer G, Marquardt JL. 1972. Retinal function in an unique syndrome of optic atrophy, juvenile diabetes mellitus, diabetes insipidus, neurosensory hearing loss, autonomic dysfunction, and hyperalanineuria. Invest Ophthalmol 11:617-624.

Nogami H, Ogasawara K, Mimura Y, Mogi K, Shutoh F, Hisano S. 2006. Developmentally-regulated expression of tissue-specific splice variant of rat vesicular glutamate transporter 1 in retina and pineal gland. J Neurochem 99:142-153.

Olavarria J. 1979. A horseradish peroxidase study of the projections from the latero-posterior nucleus to three lateral peristriate areas in the rat. Brain Res 173:137-141.

Ölveczky BP, Baccus SA, Meister M. 2003. Segregation of object and background motion in the retina. Nature 423:401-408.

Osman AA, Saito M, Makepeace C, Permutt MA, Schlesinger P, Mueckler M. 2003. Wolframin expression induces novel ion channel activity in endoplasmic reticulum membranes and increases intracellular calcium. J Biol Chem 278:52755-52762.

Paxinos G, Franklin KBJ. 2001. The mouse brain in stereotaxic coordinates. San Diego: Academic Press.

Pesch UE, Fries JE, Bette S, Kalbacher H, Wissinger B, Alexander C, Kohler K. 2004. *OPA1*, the disease gene for autosomal dominant optic atrophy, is specifically expressed in ganglion cells and intrinsic neurons of the retina. Invest Ophthalmol Vis Sci 45:4217-4225.

Peters A, Feldman ML. 1976. The projection of the lateral geniculate nucleus to area 17 of the rat cerebral cortex. I. General description. J Neurocytol 5:63-84.

Polymeropoulos MH, Swift RG, Swift M. 1994. Linkage of the gene for Wolfram syndrome to markers on the short arm of chromosome 4. Nat Genet 8:95-97.

Rando TA, Horton JC, Layzer RB. 1992. Wolfram syndrome: evidence of a diffuse neurodegenerative disease by magnetic resonance imaging. Neurology 42:1220-1224.

Reichert F, Rotshenker S. 1996. Deficient activation of microglia during optic nerve degeneration. J Neuroimmunol 70:153-161.

Roska B, Werblin F. 2001. Vertical interactions across ten parallel, stacked representations in the mammalian retina. Nature 410:583-587.

Ryan S, Arden GB. 1988. Electrophysiological discrimination between retinal and optic nerve disorders. Doc Ophthalmol 68:247-255.

Saari JC, Huang J, Possin DE, Fariss RN, Leonard J, Garwin GG, Crabb JW, Milam AH. 1997. Cellular retinaldehyde-binding protein is expressed by oligodendrocytes in optic nerve and brain. Glia 21:259-268.

Sanderson KJ, Dreher B, Gayer N. 1991. Prosencephalic connections of striate and extrastriate areas of rat visual cortex. Exp Brain Res 85:324-334.

Scolding NJ, Kellar-Wood HF, Shaw C, Shneerson JM, Antoun N. 1996. Wolfram syndrome: hereditary diabetes mellitus with brainstem and optic atrophy. Ann Neurol 39:352-360.

Sefton AJ, Dreher B. 1995. Visual System. In: Paxinos G, Editor. The rat nervous system. San Diego: Academic Press. p 833-898.

Sefton AJ, Dreher B, Lim WL. 1991. Interactions between callosal, thalamic and associational projections to the visual cortex of the developing rat. Exp Brain Res 84:142-158.

Seifert G, Schilling K, Steinhäuser C. 2006. Astrocyte dysfunction in neurological disorders: a molecular perspective. Nat Rev Neurosci 7:194-206.

Seynaeve H, Vermeiren A, Leys A, Dralands L. 1994. Four cases of Wolfram syndrome: ophthalmologic findings and complications. Bull Soc Belge Ophtalmol 252:75-80.

Shannon P, Becker L, Deck J. 1999. Evidence of widespread axonal pathology in Wolfram syndrome. Acta Neuropathol (Berl) 98:304-308.

Sharma RK, Netland PA. 2007. Early born lineage of retinal neurons express class III β-tubulin isotype. Brain Res 1176:11-17.

Sheng Z, Kawano J, Yanai A, Fujinaga R, Tanaka M, Watanabe Y, Shinoda K. 2004. Expression of estrogen receptors (α, β) and androgen receptor in serotonin neurons of the rat and mouse dorsal raphe nuclei; sex and species differences. Neurosci Res 49:185-196.

Strom TM, Hörtnagel K, Hofmann S, Gekeler F, Scharfe C, Rabl W, Gerbitz KD, Meitinger T. 1998. Diabetes insipidus, diabetes mellitus, optic atrophy and deafness (DIDMOAD) caused by mutations in a novel gene (*wolframin*) coding for a predicted transmembrane protein. Hum Mol Genet 7:2021-2028.

Takeda K, Inoue H, Tanizawa Y, Matsuzaki Y, Oba J, Watanabe Y, Shinoda K, Oka Y. 2001. WFS1 (Wolfram syndrome 1) gene product: predominant subcellular localization to endoplasmic reticulum in cultured cells and neuronal expression in rat brain. Hum Mol Genet 10:477-484.

Takei D, Ishihara H, Yamaguchi S, Yamada T, Tamura A, Katagiri H, Maruyama Y, Oka Y. 2006. WFS1 protein modulates the free Ca^{2+} concentration in the endoplasmic reticulum. FEBS Lett 580:5635-5640.

Taylor WR, Vaney DI. 2002. Diverse synaptic mechanisms generate direction selectivity in the rabbit retina. J Neurosci 22:7712-7720.

Taylor WR, Vaney DI. 2003. New directions in retinal research. Trends Neurosci 26:379-385.

Tessa A, Carbone I, Matteoli MC, Bruno C, Patrono C, Patera IP, De Luca F, Lorini R, Santorelli FM. 2001. Identification of novel WFS1 mutations in Italian children with Wolfram syndrome. Hum Mutat 17:348-349.

Ueda K, Kawano J, Takeda K, Yujiri T, Tanabe K, Anno T, Akiyama M, Nozaki J, Yoshinaga T, Koizumi A, Shinoda K, Oka Y, Tanizawa Y. 2005. Endoplasmic

reticulum stress induces Wfs1 gene expression in pancreatic β-cells via transcriptional activation. Eur J Endocrinol 153:167-176.

Voigt T. 1986. Cholinergic amacrine cells in the rat retina. J Comp Neurol 248:19-35.

Volterra A, Meldolesi J. 2005. Astrocytes, from brain glue to communication elements: the revolution continues. Nat Rev Neurosci 6:626-640.

von Gräfe A. 1858. Über die mit Diabetes vorkommenden Sehstörungen. Arch Ophthal 4:230-234.

Votruba M, Aijaz S, Moore AT. 2003. A review of primary hereditary optic neuropathies. J Inherit Metab Dis 26:209-227.

Warr WB, de Olmos JS, Heimer L. 1981. Horseradish Peroxidase: The Basic Procedure. In: Heimer L, Robards MJ, Editors. Neuroanatomical tract-tracing methods. New York: Plenum Press. p 207-262.

Wässle H. 2004. Parallel processing in the mammalian retina. Nat Rev Neurosci 5:747-757.

Watts AG, Swanson LW. 1987. Efferent projections of the suprachiasmatic nucleus: II. Studies using retrograde transport of fluorescent dyes and simultaneous peptide immunohistochemistry in the rat. J Comp Neurol 258:230-252.

Wolfram DJ, Wagener HP. 1938. Diabetes mellitus and simple optic atrophy among siblings: Report of four cases. Mayo Clin Proc 13:715-718.

Xiang M, Zhou L, Macke JP, Yoshioka T, Hendry SH, Eddy RL, Shows TB, Nathans J. 1995. The Brn-3 family of POU-domain factors: primary structure, binding specificity, and expression in subsets of retinal ganglion cells and somatosensory neurons. J Neurosci 15:4762-4785.

Yamaguchi S, Ishihara H, Tamura A, Yamada T, Takahashi R, Takei D, Katagiri H, Oka Y. 2004. Endoplasmic reticulum stress and N-glycosylation modulate expression of WFS1 protein. Biochem Biophys Res Commun 325:250-256.

Yamamoto H, Hofmann S, Hamasaki DI, Kreczmanski P, Schmitz C, Parel JM, Schmidt-Kastner R. 2006. Wolfram syndrome 1 (WFS1) protein expression in retinal ganglion cells and optic nerve glia of the cynomolgus monkey. Exp Eye Res 83:1303-1306.

Yoshida K, Watanabe D, Ishikane H, Tachibana M, Pastan I, Nakanishi S. 2001. A key role of starburst amacrine cells in originating retinal directional selectivity and optokinetic eye movement. Neuron 30:771-780.

Ziskin JL, Nishiyama A, Rubio M, Fukaya M, Bergles DE. 2007. Vesicular release of glutamate from unmyelinated axons in white matter. Nat Neurosci 10:321-330.

FIGURE LEGENDS

Fig. 1. Wfs1 protein immunoreactivity in the normal mouse brain, retina, and optic nerve. Immunoblot of extracts from the normal mouse brain, retina, and optic nerve probed with rabbit anti-mouse Wfs1 N-terminus antibody (anti-Wfs1), and with the antibody preabsorbed by incubation with GST-Wfs1 N-terminus chimeric protein (Absorbed). The arrowhead indicates Wfs1 protein bands of ~100 kDa in extracts from the brain, retina, and optic nerve (anti-Wfs1). The arrow shows a Wfs1 immunoreactive band of ~70 kDa in extracts from the retina (anti-Wfs1). These bands are not seen in the antibody-absorption experiment (Absorbed). Positions of size markers are indicated on the left.

Fig. 2. *Wfs1* mRNA signals and protein immunoreactivity in the normal mouse retina. **A-B:** Mouse *Wfs1* mRNA signals in two adjacent sections of the retina hybridized with anti-sense cRNA probes of the mouse *Wfs1* 5'-terminus (*Wfs1* AS; **A**), and with sense cRNA probes (*Wfs1* S; **B**). Arrowheads indicate moderate *Wfs1* mRNA signals in the outer row of the inner nuclear layer (INL). **C-D:** Mouse Wfs1 protein immunoreactivity in two sections of the retina immunostained with rabbit anti-mouse Wfs1 N-terminus antibody (Wfs1; **C**), and with the antibody preabsorbed by incubation with GST-Wfs1 N-terminus chimeric protein (antigen) (Abs, **D**). Arrowheads indicate Wfs1-immunoreactive neurons, of which cell bodies are weakly labeled and processes are moderately labeled, in the outer row of the INL. Note that a substantial number of *Wfs1* mRNA signals and a considerable amount of protein immunoreactivity are seen not only in the ganglion cell layer but also in the inner and the outer nuclear layers of the normal mouse retina. PR, photoreceptor; ONL, outer nuclear layer; OPL, outer plexiform layer; INL, inner nuclear layer; IPL, inner plexiform layer; GCL, ganglion cell layer; NFL, optic nerve fiber layer. Scale bars = 50 μm in **B**, and in **D** for **A**, and for **C**, respectively.

Fig. 3. Cellular localization of Wfs1 in the inner nuclear layer of the normal mouse retina. **A-C**: Wfs1 immunoreactivity in horizontal cells. A retinal section was double-immunostained for Wfs1 (Wfs1; **A**; Alexa® Fluor™ 488 label; green) and for a horizontal cell marker (Calbindin-D-28K, CalD28K, **B**; Alexa® Fluor™ 594 label; red). Cell nuclei are labeled in blue with bisBenzimide (Hoechst 33258; **B, C**). Panel **C** is an overlaid image. Arrows indicate a horizontal cell immunoreactive for Wfs1. **D-F**: Wfs1 immunoreactivity in bipolar cells. A retinal section was double-immunostained for Wfs1 (Wfs1; **D**; Alexa® Fluor™ 488 label; green) and for a bipolar cell marker (G-protein Goα, Goα, **E**; Alexa® Fluor™ 594 label; red). Cell nuclei are labeled in blue with bisBenzimide (Hoechst 33258; **E, F**). Panel **F** is an overlaid image. Arrows, and arrowheads show a putative ON-cone bipolar, and a rod bipolar cells that are immunoreactive for Wfs1, respectively. **G-I**: A control experiment of Wfs1 immunoreactivity in bipolar cells. An adjacent retinal section of panels **D-F** was double-immunostained for Wfs1 after a preabsorption procedure (Wfs1 Abs; **G**; Alexa® Fluor™ 488 label; green) and for Goα (**H**; Alexa® Fluor™ 594 label; red). Cell nuclei are labeled in blue with bisBenzimide (Hoechst 33258; **H, I**). Panel **I** is an overlaid image. Arrows, and arrowheads show a putative ON-cone bipolar, and a rod bipolar cells that are not immunoreactive for Wfs1, respectively. **J-O**: Wfs1 immunoreactivity in non-displaced amacrine cells. A retinal section was double-immunostained for Wfs1 (Wfs1; **J**; Alexa® Fluor™ 488 label; green) and for a non-displaced amacrine cell marker (Choline acetyltransferase, ChAT, **K**; Alexa® Fluor™ 594 label; red). Another section was double-immunostained for Wfs1 (Wfs1; **M**; Alexa® Fluor™ 488 label; green) and for another non-displaced amacrine cell marker (Calbindin-D-28K, CalD28K, **N**; Alexa® Fluor™ 594 label; red). Cell nuclei are labeled in blue with bisBenzimide (Hoechst 33258; **N, O**). Panels **L** and **O** are overlaid images. Arrowheads indicate non-displaced amacrine cells immunoreactive

for Wfs1. These fluorescence photomicrographs were taken with a FV500 confocal microscope (Olympus, Tokyo, Japan). Note that Wfs1 immunoreactivity is observed in photoreceptors, horizontal cells, bipolar cells, and in non-displaced amacrine cells. ONL, outer nuclear layer; OPL, outer plexiform layer; INL, inner nuclear layer; IPL, inner plexiform layer; GCL, ganglion cell layer. Scale bar = 20 μm in **O** for **A-N**.

Fig. 4. Cellular localization of Wfs1 in the ganglion cell layer of the normal mouse retina. **A-F**: Wfs1 immunoreactivity in displaced amacrine cells. A whole-mount retina (**A-C**) and a vertical retinal section (**D-F**) were double-immunostained for Wfs1 (Wfs1; **A, D**; Alexa® Fluor™ 488 label; green) and for a displaced amacrine cell marker (Choline acetyltransferase, ChAT, **B, E**; Alexa® Fluor™ 594 label; red). Cell nuclei are labeled in blue with bisBenzimide (Hoechst 33258; **B, C, E, F**). Panels **C** and **F** are overlaid images. Arrowheads indicate displaced amacrine cells immunoreactive for Wfs1. **G-I**: Wfs1 immunoreactivity in retinal ganglion cells (RGCs). Panels show a retinal section in which Wfs1 (**G**; Alexa® Fluor™ 488 label; green) and Fluorescent Latex Microspheres (FLM; **H**; rhodamine label; red) double labeling was made. Cell nuclei are labeled in blue with bisBenzimide (Hoechst 33258; **H, I**). Panel **I** is an overlaid image. Arrows indicate a retinal ganglion cell immunoreactive for Wfs1. **J-L**: A control experiment of Wfs1 immunoreactivity in RGCs. Wfs1 (**J**; Alexa® Fluor™ 488 label; green) and FLM (**K**; rhodamine label; red) double labeling was performed in an adjacent retinal section of panels G-I. Cell nuclei are labeled in blue with bisBenzimide (Hoechst 33258; **K, L**). Panel **L** is an overlaid image. Arrows indicate a retinal ganglion cell not immunoreacitve for Wfs1. **M-R**: Wfs1 immunoreactivity in RGCs analyzed by double immunohistochemistry. A retinal section was double-immunostained for Wfs1 (Wfs1; **M**; Alexa® Fluor™ 488 label; green) and for a ganglion cell marker (Tubulin βIII isoform, Tubulin βIII, **N**; Alexa® Fluor™ 594 label; red). Another

section was double-immunostained for Wfs1 (Wfs1; **P**; Alexa® Fluor™ 488 label; green) and for another ganglion cell marker (Brn-3a POU-domain transcription factor, Brn-3a, **Q**; Alexa® Fluor™ 594 label; red). Cell nuclei are labeled in blue with bisBenzimide (Hoechst 33258; **N, O, Q, R**). Panels **O** and **R** are overlaid images. Arrows indicate RGCs immunoreactive for Wfs1. These fluorescence photomicrographs were taken with a FV500 confocal microscope (Olympus, Tokyo, Japan). Note that Wfs1 immunoreactivity is observed in both displaced amacrine cells and RGCs. IPL, inner plexiform layer; GCL, ganglion cell layer; NFL, optic nerve fiber layer. Scale bar = 20 μm in **R** for **A-Q**.

Fig. 5. Wfs1 immunoreactivity in retinal ganglion cells (**A-C**) and in Müller cells **(D-F)** of the normal mouse retina. **A-C**: Wfs1 (**A**; Alexa® Fluor™ 488 label; green) and Fluoro-Ruby (**B**; tetramethylrhodamine label; red) double labeling. Panel **C** is an overlaid image. Arrows indicate a retinal ganglion cell immunoreactive for Wfs1. **D-F**: Double immunostaining for Wfs1 (Wfs1; **D**; Alexa® Fluor™ 488 label; green) and for a Müller cell marker (glutamine synthetase, GS, **E**; Alexa® Fluor™ 594 label; red). Panel **F** is an overlaid image. Arrows, and arrowheads show a cell body, and an inner process of Müller cells immunoreactive for Wfs1, respectively. Note that Wfs1 immunoreactivity is observed in Müller cells as well as in neurons of the retina. These fluorescence photomicrographs were taken with a LSM 510 confocal microscope (Carl Zeiss Jena GmbH, Jena, Germany). ONL, outer nuclear layer; OPL, outer plexiform layer; INL, inner nuclear layer; IPL, inner plexiform layer; GCL, ganglion cell layer. Scale bars = 20 μm in **C** for **A-B**, 50 μm in **F** for **D-E**.

Fig. 6. Distribution of glial cells in the normal mouse optic nerve. Panels show double immunostaining for two glial cell markers, glial fibrillary acidic protein (GFAP, **A**; Alexa® Fluor™ 488 label; green), and glutamine synthetase (GS, **B**; Alexa® Fluor™ 594 label; red).

Panel **C** is an overlaid image. The mouse optic nerve is divided into three parts: intraretinal (i), astrocytic filament dense (afd), and astrocytic filament sparse (afs). Arrows, and arrowheads indicate the border between i and afd, and the boundary between afd and afs, respectively. These fluorescence photomicrographs were taken with a FV500 confocal microscope (Olympus, Tokyo, Japan). Note that the area containing GS-immunoreactive cells in the mouse optic nerve corresponds to the afs part. Scale bars = 100 μm in **C** for **A-B**.

Fig. 7. *Wfs1* mRNA signals and protein immunoreactivity in the normal mouse optic nerve. **A-B:** Mouse *Wfs1* mRNA signals in two adjacent sections of the optic nerve hybridized with anti-sense cRNA probes of the mouse *Wfs1* 5'-terminus (*Wfs1* AS; **A**), and with sense cRNA probes (*Wfs1* S; **B**). **C-D:** Mouse Wfs1 protein immunoreactivity in two adjacent sections of the optic nerve immunostained with rabbit anti-mouse Wfs1 N-terminus antibody (Wfs1; **C**), and with the antibody preabsorbed by incubation with GST-Wfs1 N-terminus chimeric protein (antigen) (Abs; **D**). **E-F:** Higher magnification photomicrographs of mouse Wfs1 immunoreactivity in another adjacent section of panel **C**. Panels **E**, and **F** show Wfs1-immunoreactive cells in the astrocytic filament dense (afd) part, and those in the astrocytic filament sparse (afs) part, respectively. Note that both *Wfs1* mRNA signals and Wfs1 protein immunoreactivity are present in the mouse optic nerve. Scale bars = 200 μm in **D** for **A-C**, 50 μm in **F** for **E**.

Fig. 8. Cellular localization of Wfs1 in the normal mouse optic nerve. **A-I**: Double immunostaining for Wfs1 (Wfs1; **A**, **D**, **G**; Alexa® Fluor™ 488 label; green) and for an astrocyte marker (glial fibrillary acidic protein, GFAP, **B**, **E**, **H**; Alexa® Fluor™ 594 label; red). Cell nuclei are labeled in blue with bisBenzimide (Hoechst 33258). Panels **C**, **F**, and **I** are overlaid images. Arrows, and arrowheads in **A-C** indicate the border between intraretinal

(i) and astrocytic filament dense (afd) parts, and the boundary between the afd and astrocytic filament sparse (afs) parts, respectively. Panels **D-F**, and **G-I** are higher mignification photomicrographs of the afd, and afs parts, respectively. These panels show that Wfs1 immunoreactivity is observed in astrocytes. **J-O**: Double immunostaining for Wfs1 (Wfs1; **J, M**; Alexa® Fluor™ 488 label; green) and for an oligodendrocyte marker (RIP, **K, N**; Alexa® Fluor™ 594 label; red). Cell nuclei are labeled in blue with bisBenzimide (Hoechst 33258). Panels **L** and **O** are overlaid images. Panels **M-O** are higher magnification photomicrographs of the afs part. These panels show that Wfs1 immunoreactivity is not seen in oligodendrocytes. **P-R**: Double immunostaining for Wfs1 (Wfs1; **P**; Alexa® Fluor™ 488 label; green) and for a glial cell marker (glutamine synthetase, GS, **Q**; Alexa® Fluor™ 594 label; red). Panel **R** is an overlaid image. Arrows, and arrowheads indicate the border between i and afd parts, and the boundary between the afd and afs parts, respectively. Insets are higher magnification photomicrographs around the boundary between the afd and afs parts. These panels and insets show that colocalization of Wfs1 immunoreactivity and GS immunoreactivity is not seen in the optic nerve but in the retina. These fluorescence photomicrographs were taken with FV500 (Olympus, Tokyo, Japan; **A-O**), and with LSM 510 (Carl Zeiss Jena GmbH, Jena, Germany; **P-R**) confocal microscopes. Scale bars = 100 μm in **C** for **A-B**, and for **J-L**, 20 μm in **O** for **D-I**, and for **M-N**, 200 μm in **R** for **P-Q**, 20 μm in inset of **R** for insets of **P-Q**.

Fig. 9. *Wfs1* mRNA signals and protein immunoreactivity in the normal mouse brain. **A-C:** Mouse *Wfs1* mRNA signals (*Wfs1* mRNA, **A**), mouse Wfs1 protein immunoreactivity (Wfs1, **B**), and cytoarchitecture (Nissl, **C**) in three serial sections of the visual cortex hybridized with anti-sense cRNA probes of the mouse *Wfs1* 5'-terminus, immunostained with rabbit anti-mouse Wfs1 N-terminus antibody, and Nissl-stained with cresyl violet, respectively. Short

lines in **B** and **C** indicate borders between each cortical area. These panels show that both *Wfs1* mRNA signals and Wfs1 immunoreactivity are observed in layer II of the visual cortex. V1, primary visual cortex; V2L, lateral area of the secondary visual cortex; V2ML, mediolateral area of the secondary visual cortex; V2MM, mediomedial area of the secondary visual cortex; CA1, CA1 field of the hippocampus; I, layer I; II, layer II; III, layer III; IV, layer IV; V, layer V; VI, layer VI. **D-F:** Mouse *Wfs1* mRNA signals (*Wfs1* mRNA, **D**), mouse Wfs1 protein immunoreactivity (Wfs1, **E**), and cytoarchitecture (Nissl, **F**) in three serial sections of the superior colliculus (SC). Dashed lines in **F** indicate borders of each superior collicular layer, and the boundary of the periaqueductal gray (PAG). These panels show that *Wfs1* mRNA signals and Wfs1 immunoreactivity are seen in the zonal (Zo), superficial gray (SuG), and intermediate gray (InG) layers of the SC. Op, optic nerve layer of the SC; InWh, intermediate white layer of the SC; DpG, deep gray layer of the SC. Scale bar = 500 μm in **F** for **A-E**.

Fig. 10. Wfs1 protein immunoreactivity in the normal mouse suprachiasmatic nucleus (SCN), optic chiasm (OX), and optic tract (OT). **A-B:** Mouse Wfs1 protein immunoreactivity in two adjacent sections of the SCN immunostained with rabbit anti-Wfs1 N-terminus antibody (Wfs1, **A**), and with the antibody preabsorbed by incubation with GST-Wfs1 N-terminus chimeric protein (antigen) (Abs, **B**). The dashed lines indicate the boundary of the SCN. These panels show that moderate Wfs1 immunoreactivity is seen in the SCN. maOT, medial accessory optic tract. **C-D:** Mouse Wfs1 protein immunoreactivity in the OX (**C**) and OT (**D**). These panels show that Wfs1 immunoreactivity is not seen in the OX or OT. SON, supraoptic nucleus. Scale bar = 200 μm in **D** for **A-C**.

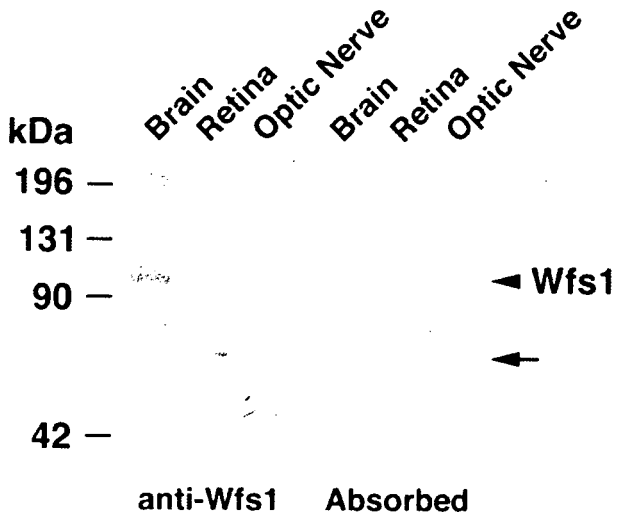

Figure 1 Kawano et al.

Figure 1. Wfs1 protein immunoreactivity in the normal mouse brain, retina, and optic nerve.

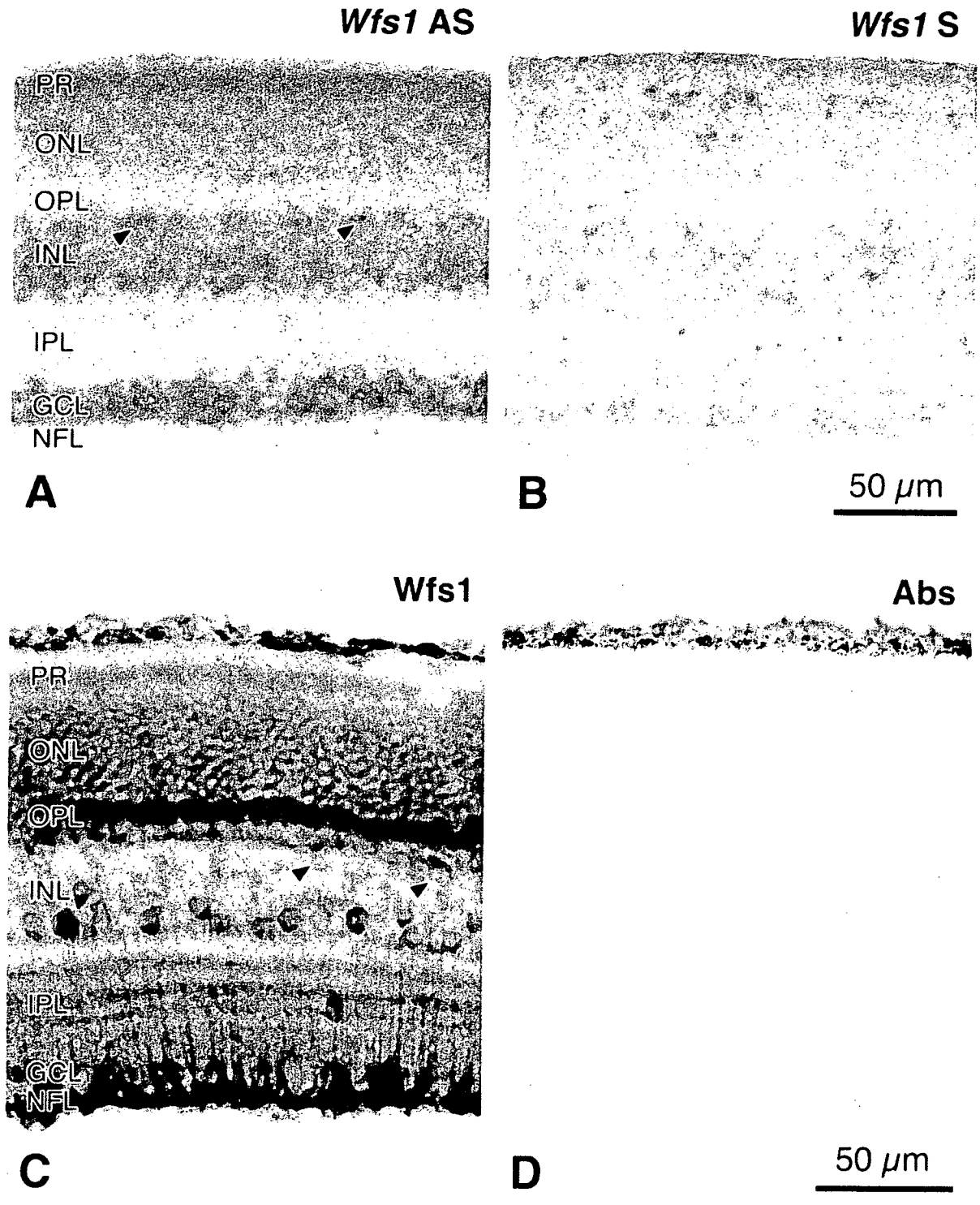

Figure 2 Kawano et al.

Figure 2. *Wfs1* mRNA signals and protein immunoreactivity in the normal mouse retina.

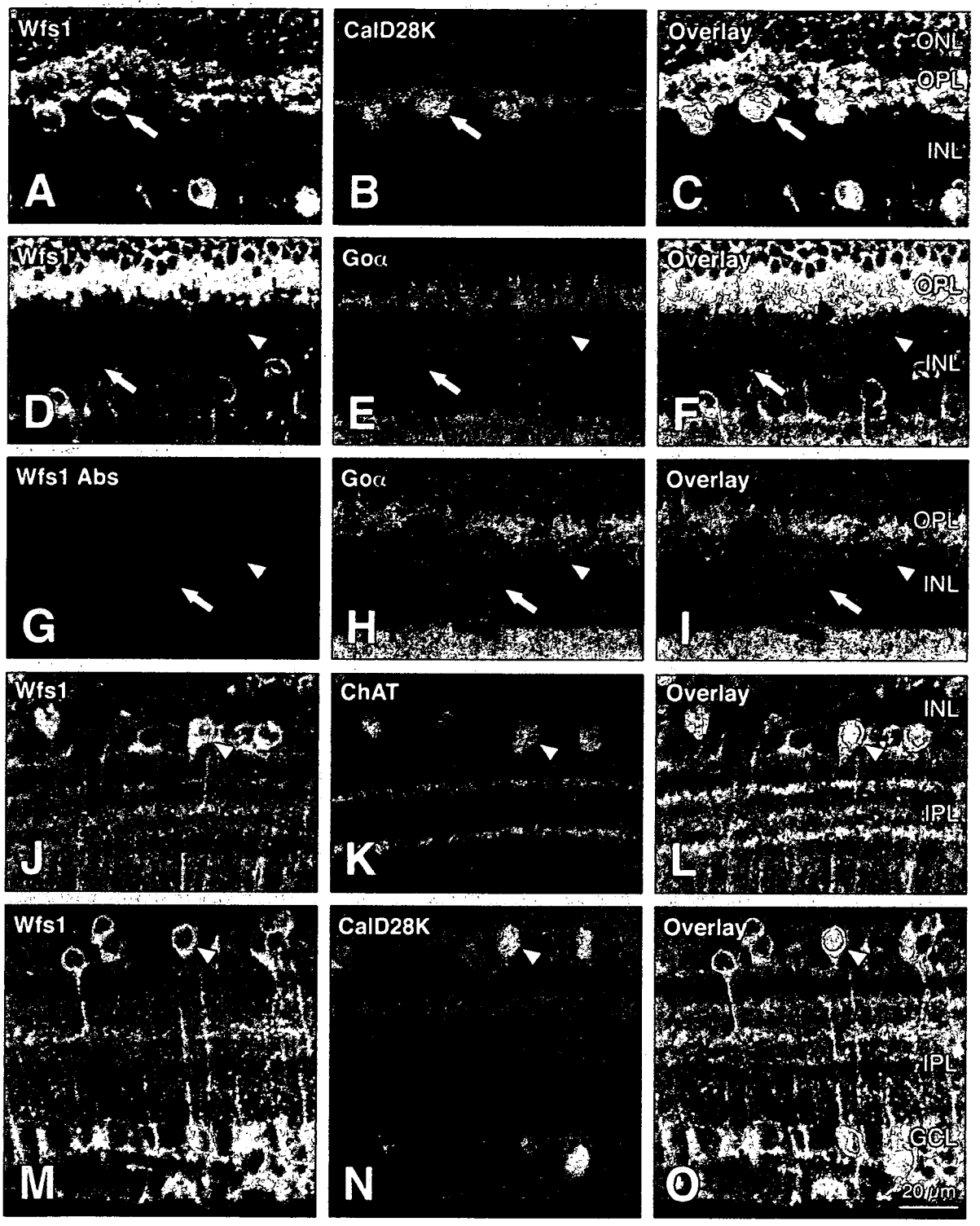

Figure 3 Kawano et al.

Figure 3. Cellular localization of Wfs1 in the inner nuclear layer of the normal mouse retina.

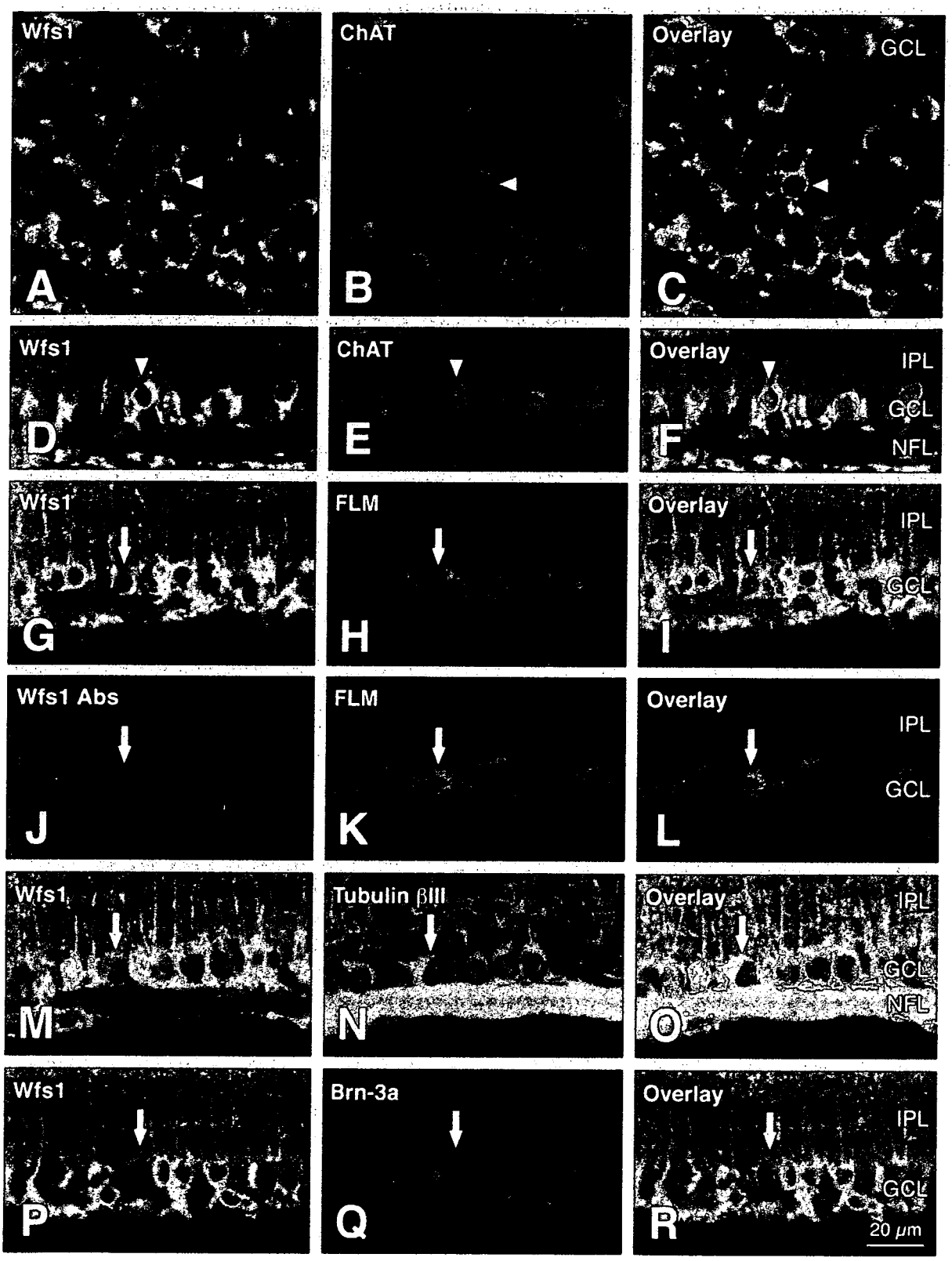

Figure 4 Kawano et al.

Figure 4. Cellular localization of Wfs1 in the ganglion cell layer of the normal mouse retina.

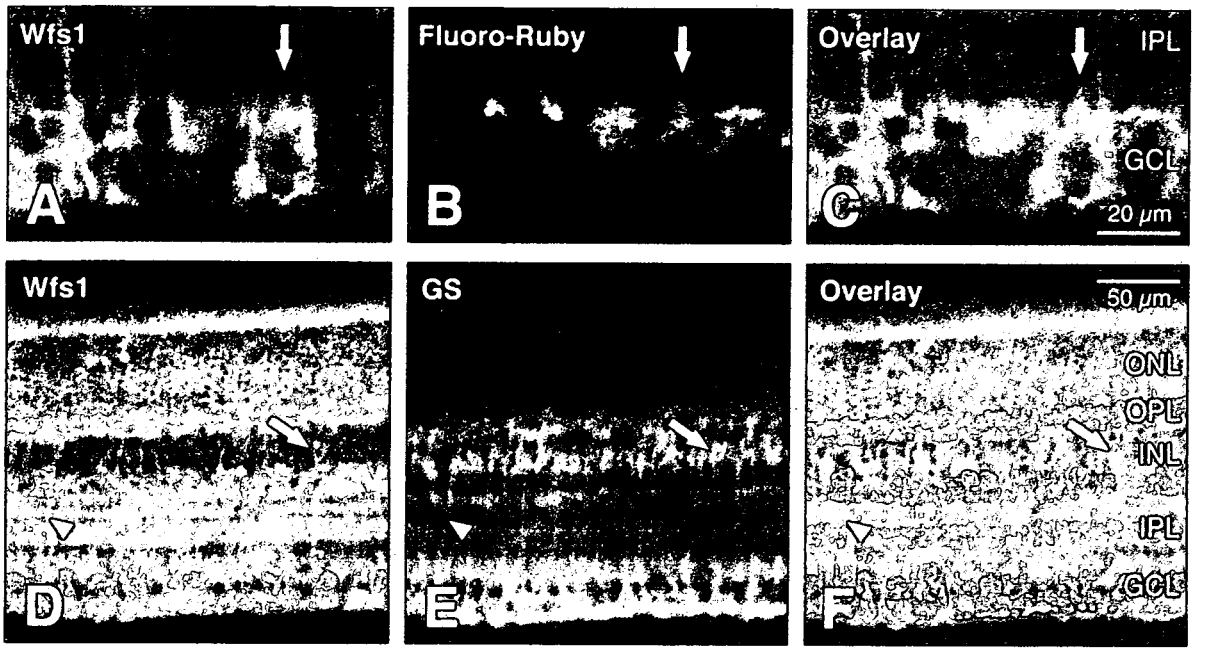

Figure 5 Kawano et al.

Figure 5. Wfs1 immunoreactivity in retinal ganglion cells (**A-C**) and in Müller cells (**D-F**) of the normal mouse retina.

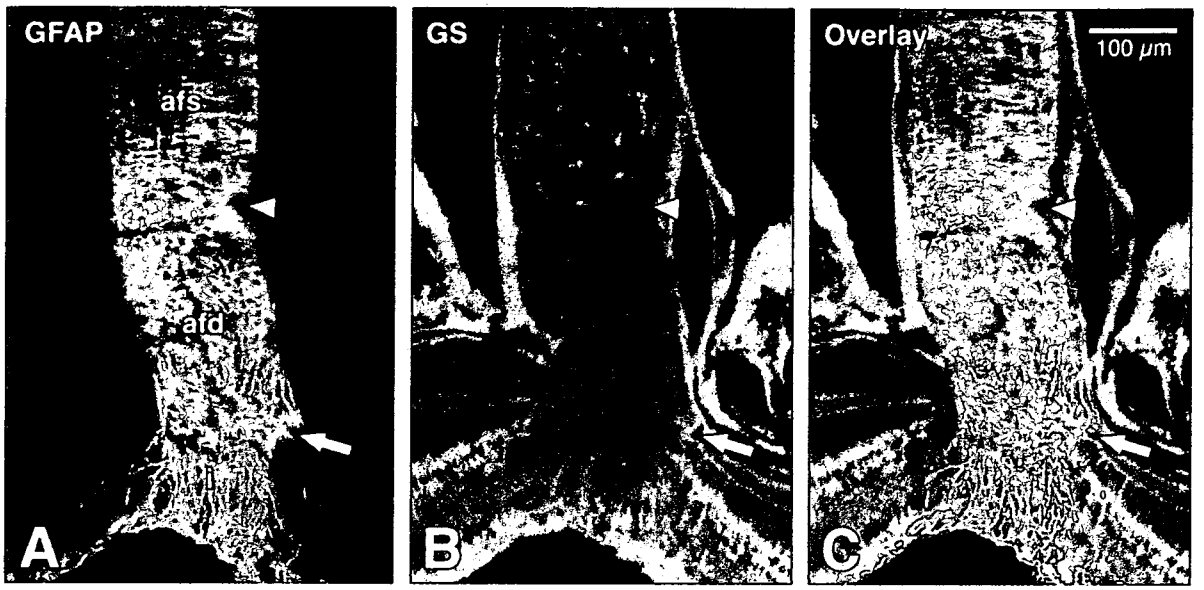

Figure 6. Distribution of glial cells in the normal mouse optic nerve.

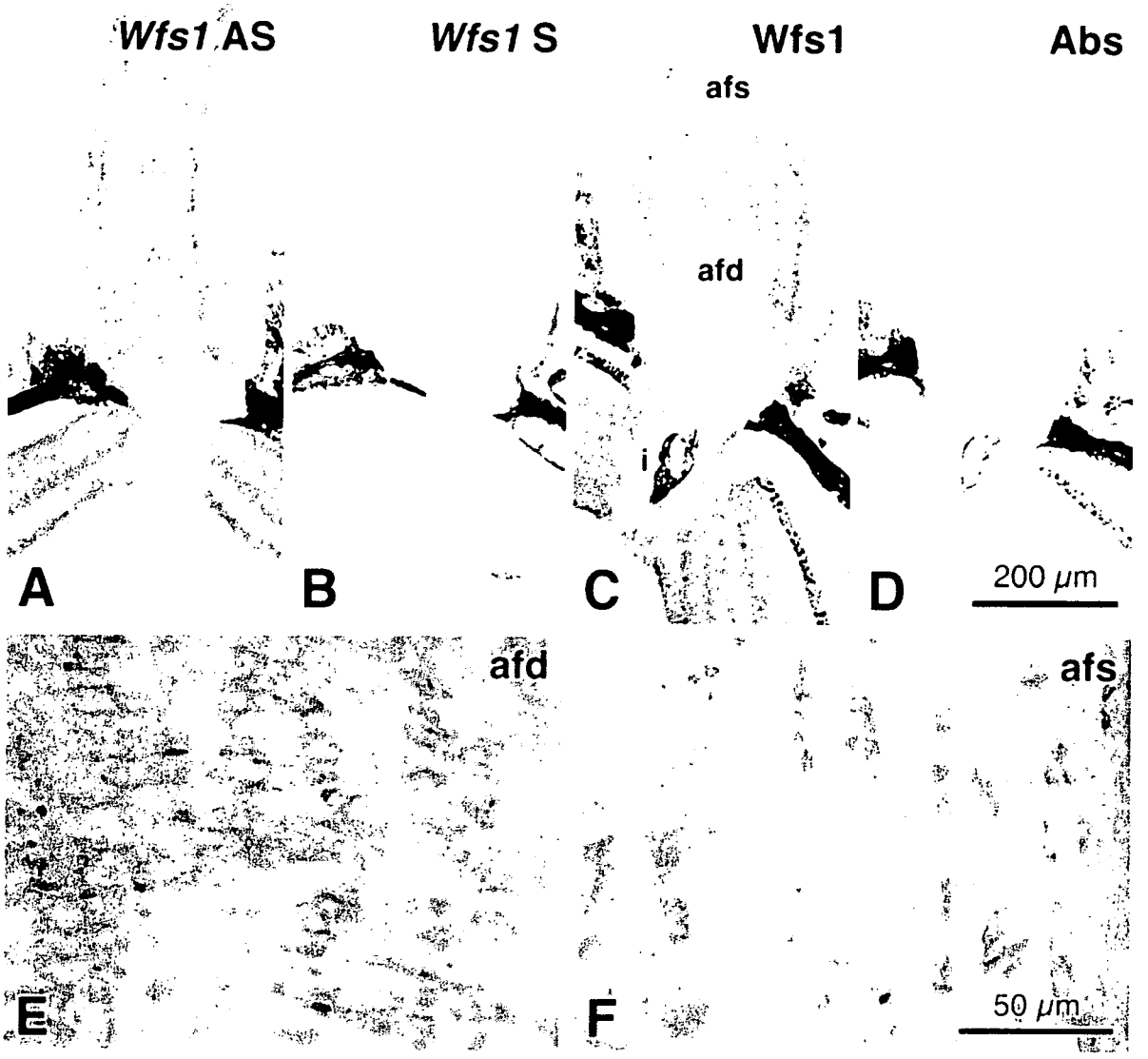

Figure 7. *Wfs1* mRNA signals and protein immunoreactivity in the normal mouse optic nerve.

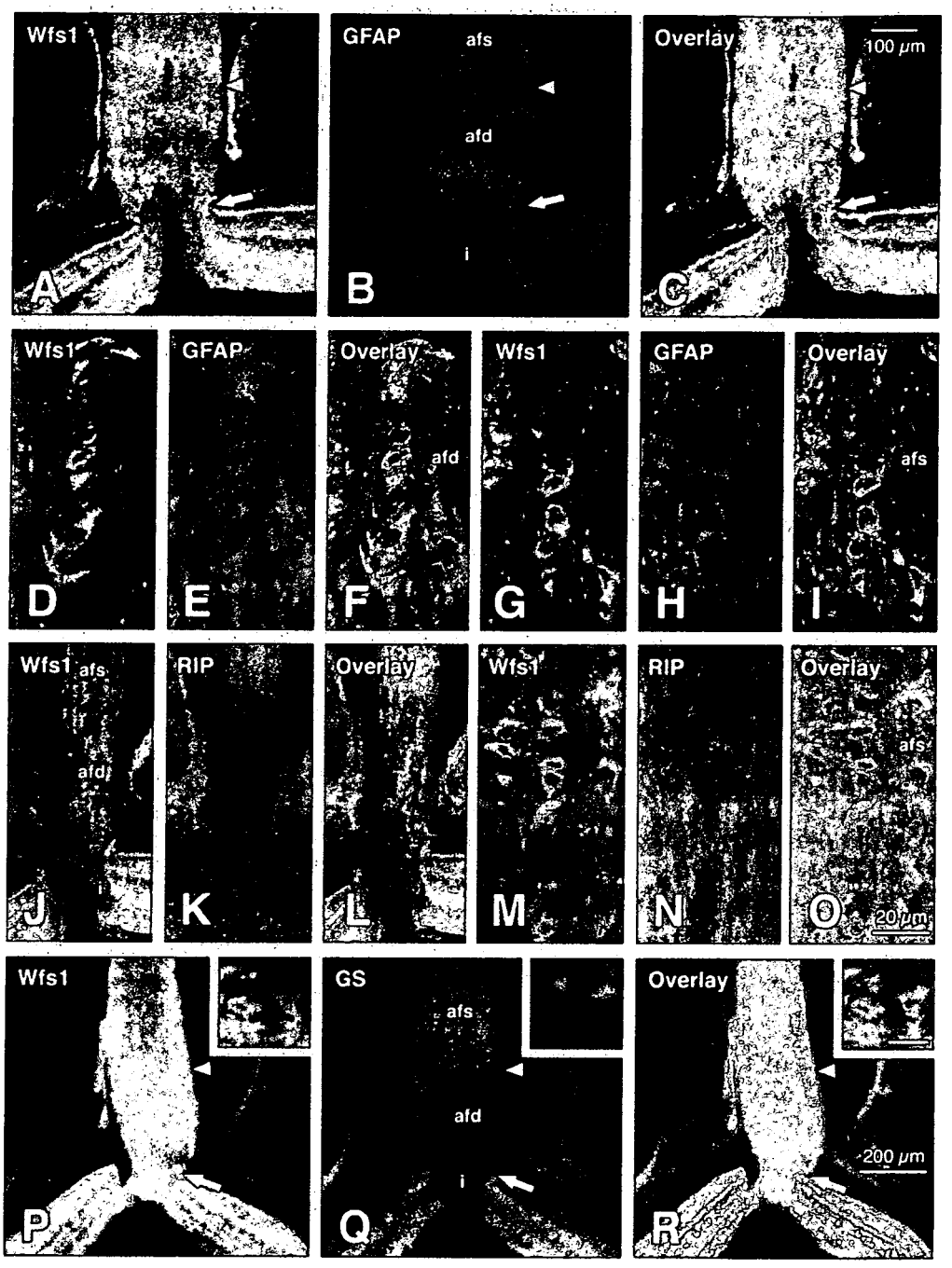

Figure 8. Cellular localization of Wfs1 in the normal mouse optic nerve.